CHEMISTRY OF MATERIALS

Article

pubs.acs.org/cm

Ladder-Type Nonacyclic Structure Consisting of Alternate Thiophene and Benzene Units for Efficient Conventional and Inverted Organic Photovoltaics

Yen-Ju Cheng,* Chiu-Hsiang Chen, Yu-Shun Lin, Chih-Yu Chang, and Chain-Shu Hsu*

Department of Applied Chemistry, National Chiao Tung University, 1001 Ta Hsueh Road, Hsin-Chu, 30010 Taiwan

Supporting Information

ABSTRACT: A ladder-type nonacyclic thienyl-phenylene-thienylene-phenylene-thienyl **TPTPT** unit, consisting of alternate interfused thiophene and benzene units, is designed and synthesized. This multifused distannyl-**TPTPT** monomer was polymerized with two electron-deficient acceptors, 4,7-dibromo-2,1,3-benzothiadiazole **BT** and 5,8-dibromo-2,3-diphenylquinoxaline **QX** monomers, by Stille coupling reaction to afford two alternating donor−acceptor copolymers, **PTPTPTBT** and **PTPTPTQX**, respectively. Because of the covalent planarization of the conjugated framework, **PTPTPTBT** simultaneously possess excellent solubilities for solution-processability, low bandgaps with suitable position of HOMO/LUMO energy levels, and high hole mobilities. The devices based on the **PTPTPTBT**/$PC_{71}BM$ blend not only showed a promising PCE of 5.3% with conventional configuration but also achieved a high PCE of 5.9% with inverted configuration. This value is among the highest performance from the inverted solar cells incorporating a donor−acceptor low bandgap polymer.

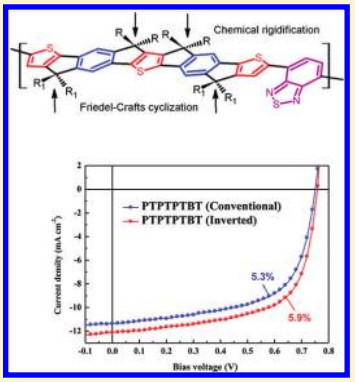

KEYWORDS: *ladder-type structure, organic photovoltaics, alternating copolymer*

INTRODUCTION

Research on excitonic solar cells using organic p-type (donor) and n-type (acceptor) semiconductors has attracted tremendous scientific and industrial interest in recent years.[1] The most critical challenge at molecular level is to translate excellent microscopic properties of photoactive materials into optimal macroscopic device characteristics.[2] Donor−acceptor (D−A) polymers incorporating tricyclic 2,7-fluorene unit have shown to possess deep-lying HOMO energy levels that are an important prerequisite to guarantee greater open-circuit voltages (V_{oc}).[3] Nevertheless, because of high aromatic stabilization energy of the benzene rings, fluorene-based polymers exhibit relatively large optical band gaps (>2 eV) that restrict their absorption ability and, thus, result in insufficient photocurrents. 4*H*-cyclopentadithiophene (**CPDT**) appears to be another attractive thiophene-based tricyclic analogue. **CPDT**-based D−A polymers have shown narrower optical bandgaps and higher hole mobilities, yielding very high short-circuit currents (J_{sc}).[4] Unfortunately, the resulting devices deliver only moderate V_{oc} values (<0.65 V). Development of a new donor moiety that can extract the advantages of benzene-based fluorene and thiophene-based **CPDT** units may overcome the trade-off between J_{sc} and V_{oc}. Chemical planarization by covalently fastening adjacent aromatic units in the polymeric backbone can facilitate π-electron delocalization and increase effective conjugation length.[5] Moreover, such rigidification also suppresses the rotational disorder around interannular single bonds and lowers the reorganization energy, which in turn enhances the intrinsic charge mobility.[6] On the basis of the aforementioned consideration, integration of alternate thiophene and benzene units into a coplanar entity with forced rigidification becomes a novel molecular design. Pentacyclic fused indacenodithiophene (**IDT**) unit exemplifies a successful system in this category. The devices utilizing the **IDT**-based D−A polymers have shown superior photovoltaic performance.[7] The other pentacyclic arrangement system is the fused diindenothiophene (**DIDT**) with highly planar structure. We recently reported a **DIDT**-based alternating copolymer poly(**DIDT**-*alt*-dithienylbenzothiadiazole) (**PDIDTDTBT**) and its corresponding device has shown a moderate power conversion efficiency (PCE) of 1.65% (Figure 1).[8] If the 3,7-position of the **DIDT** units in **PDIDTDTBT** are covalently rigidified with the 3-position of two adjacent thiophene rings by a carbon bridge, an alternate thienyl-phenylene-thienylene-phenylene-thienyl (**TPTPT**) nonacylic building block with forced coplanarity will be emerged (Figure 1). Compared to **DIDT**, **TPTPT** unit may exhibit improved optical and electronic properties due to the higher thiophene content and extended coplanarity of the conjugated backbone. In this research, we report the synthesis of the distannyl-**TPTPT** monomer which is copolymerized with 4,7-dibromo-2,1,3-benzothiadiazole **BT** and 5,8-dibromo-2,3-diphenylquinoxaline **QX** acceptor monomers to afford two alternating D−A copolymers poly(**TPTPT**-*alt*-benzothiadia-

Received: September 1, 2011
Revised: October 3, 2011
Published: October 19, 2011

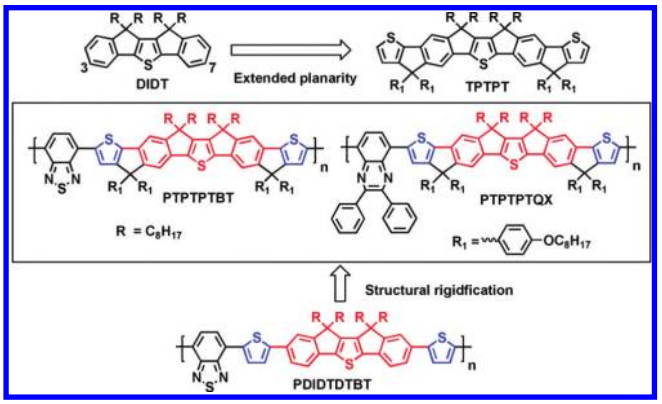

Figure 1. Chemical structure of **DIDT** and **TPTPT** units, fused **PTPTPTBT**, **PTPTPTQX** copolymers, and nonfused **PDIDTDTBT**.

zole) (**PTPTPTBT**) and poly(**TPTPT**-*alt*-quinoxaline) (**PTPTPTQX**), respectively (Figure 1). Bulk-heterojunction (BHJ) solar cells incorporating these polymers have shown promising photovoltaic performance in both conventional and inverted architectures.

RESULTS AND DISCUSSION

Synthesis. The synthetic route toward Sn-**TPTPT** monomer is depicted in Scheme 1. Suzuki coupling of 2, 8-diboronic ester **DIDT** (**1**) with ethyl 2-bromothiophene-3-carboxylate yielded compound **2**. Double nucleophilic addition of the ester groups in **2** by (4-octyloxy)phenyl magnesium bromide led to the formation of benzylic alcohols in **3** which was subjected to intramolecular Friedel–Crafts cyclization under acidic condition to furnish the nonacyclic arene **TPTPT** in a high yield of 81%. It is noteworthy that the reaction sites occur regioselectively at 3,7-position of **DIDT** unit. **TPTPT** can be efficiently lithiated by *t*-butyllithium followed by quenching with trimethyltin chloride to afford the distannyl Sn-**TPTPT** in a moderate yield of 62%. 2,7-dibromo-2,1,3-benzothiadiazole (**BT**) and 5,8-dibromo-2,3-diphenylquinoxaline (**QX**) were copolymerized with the donor Sn-**TPTPT** by Stille coupling to afford **PTPTPTBT** (M_n = 30 kDa, PDI = 1.69) and **PTPTPTQX** (M_n = 34 kDa, PDI = 1.60), respectively.

These copolymers purified by successive reprecipitation and Soxhlet extraction showed narrow molecular weight distributions with polydispersity index below 1.7. The resulting copolymers flanked with eight side chains on **TPTPT** showed excellent solubilities in common organic solvents, such as chloroform, toluene, chlorobenzene, and 1,2-dichlorobenzene.

Thermal Properties. Thermal stability of **PTPTPTBT** and **PTPTPTQX** was analyzed by thermal gravimetric analysis (TGA). The decomposition temperatures (T_d) of **PTPTPTBT** and **PTPTPTQX** are located at 389 and 409 °C (Figure 2), indicating sufficient thermal stabilities for PSCs applications. From the DSC measurement, both of the polymers showed neither glass transition temperature nor melting point, suggesting that these copolymers tend to be amorphous (Table 1).

Optical Properties. The optical properties of the polymers are shown in Table 2. Both of **PTPTPTBT** and **PTPTPTQX**

Scheme 1. Synthetic Route of the Sn-TPTPT Monomer Leading to the Targeted PTPTPTBT and PTPTPTQX Copolymers

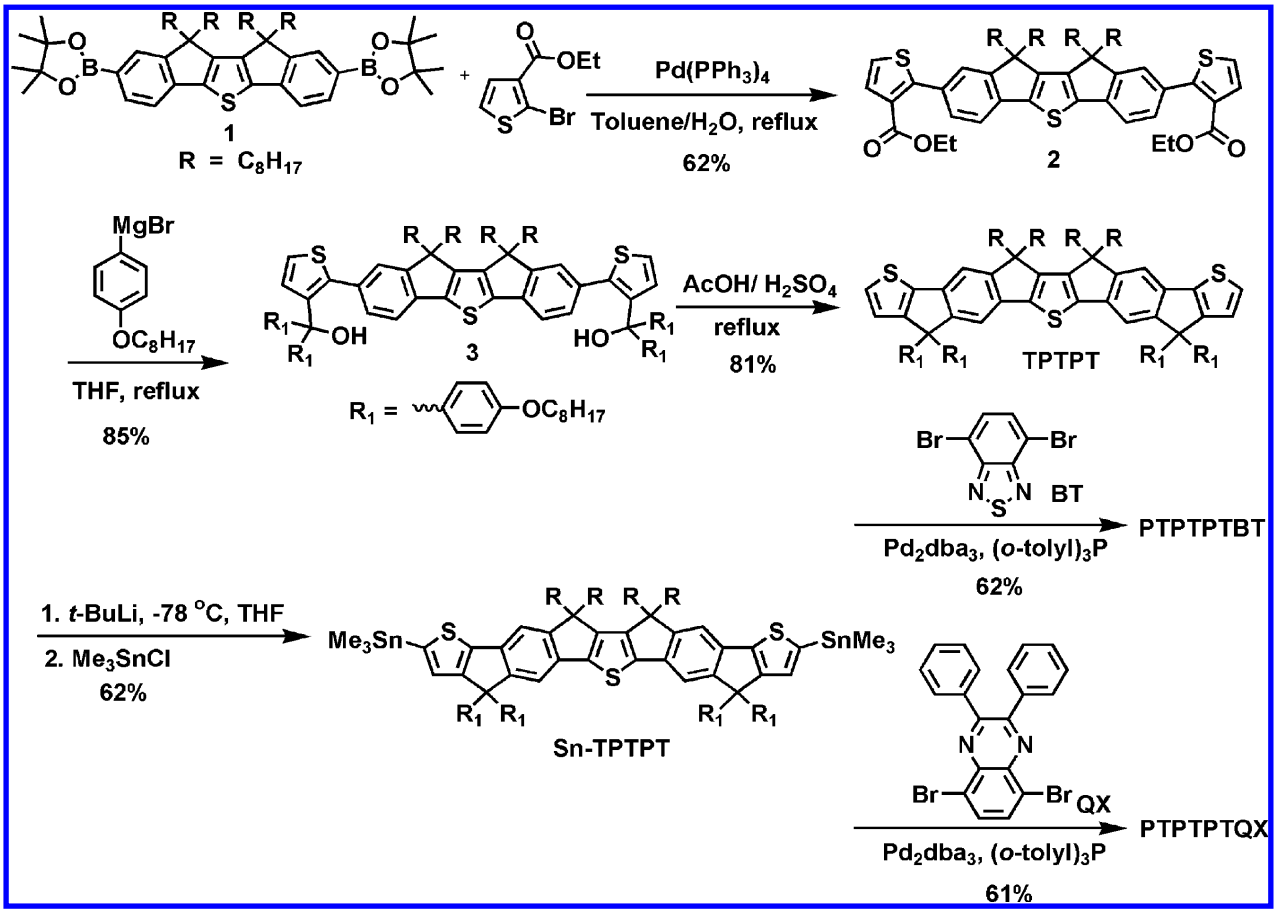

dx.doi.org/10.1021/cm202612t|*Chem. Mater.* 2011, 23, 5068–5075

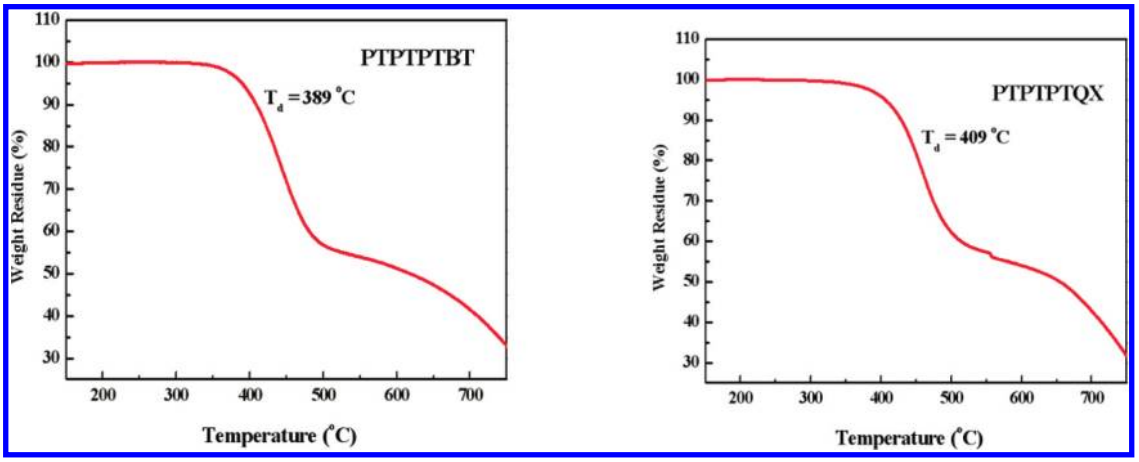

Figure 2. Thermogravimetric analysis (TGA) of **PTPTPTBT** and **PTPTPTQX**.

Table 1. Molecular Weights and Thermal Properties of Polymers

copolymer	M_w	M_n	PDI	T_g (°C)	T_d (°C)[a]
PTPTPTBT	50700	30000	1.69		389
PTPTPTQX	54400	34000	1.60		409

[b]Decomposition temperature (5% weight loss) measured by TGA.

Table 2. Optical Properties of the Copolymers

	chloroform solution			thin film		
polymer	λ_{max} (nm)	λ_{onset} (nm)	E_g^{opt} (eV)	λ_{max} (nm)	λ_{onset} (nm)	E_g^{opt} (eV)
PTPTPTBT	444, 628	713	1.74	452, 639	715	1.73
PTPTPTQX	449, 593	674	1.84	452, 593	688	1.80

exhibited two distinct bands in the absorption spectra (Figure 3). One band at shorter wavelengths region is due to localized $\pi-\pi^*$ transitions and the other band at longer wavelengths is attributed to intramolecular charge transfer (ICT). Compared to **PTPTPTQX** showing the absorption maxima at 452 and 593 nm in the thin film, **PTPTPTBT** exhibited a similar absorption maximum at 452 nm but a bathochromic shift of the ICT band at 639 nm. In addition, the optical band gaps (E_g^{opt}) deduced from the absorption edges of thin film spectra are determined to be 1.73 eV (715 nm) for **PTPTPTBT** and 1.80 eV (688 nm) for **PTPTPTQX**. These results indicate that accepting strength of **BT** is stronger than that of **QX** unit. It should be emphasized that **PTPTPTBT** showed significantly red-shifted absorption maximum in comparison with its corresponding nonfused **PDIDTDTBT** analogue (444 vs 415 nm for the localized transition and 628 vs 544 nm for the ICT transition in chloroform solution), demonstrating that the effective conjugated length of the coplanar donor is increased and electron coupling between the rigidified donor and the acceptor units is substantially enhanced. Note that the intensities of the shorter wavelength bands of the polymer in the solid state are apparently stronger than those in the solution state, which also suggests that the rigid and coplanar nonacyclic units can enhance their light absorption ability in the solid state.

Theoretical Calculations. To further understand the effect of covalent planarization on the molecular structures and properties, we performed theoretical calculations by density functional theory at the level of B3LYP/6-31G(d). One repeating units **TPTPTBT** and **DIDTDTBT** were used as simplified models for simulation of PT**PTPTBT** and P**DIDTDTBT** copolymers, respectively. All the side-chain substituents were replaced with methyl groups for simplicity. The optimized structures for **TPTPTBT** and **DIDTDTBT** are shown in Figure 4. The strategy to sew-up C64/C65 and C61/C62 of **DIDTDTBT** effectively planarizes the whole molecule (**TPTPTBT**), in which the dihedral angels φ(C42−C43−C44−C45) and φ(C55−C54−C60−C61) are zero. For comparison, the corresponding angles in **DIDTDTBT** are φ(C64−C25−C24−C65) = 26.6° and φ(C62−C34−C39−C61) = 23.6°. Furthermore, such ring-fusion also makes impact on the coplanarity between the **BT** and the neighboring thiophene rings: the dihedral angles between these two

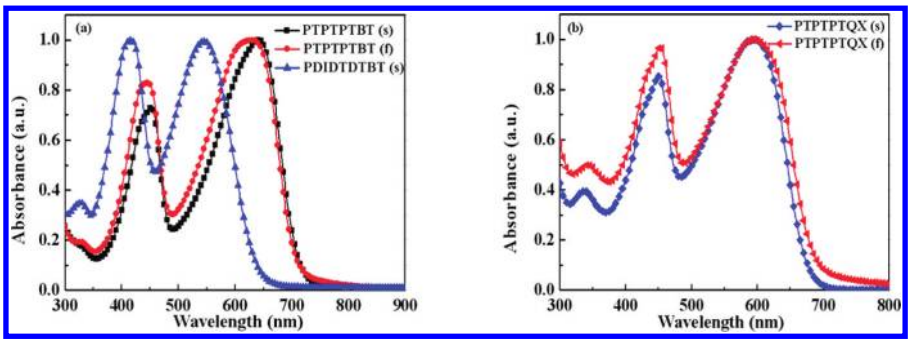

Figure 3. Normalized absorption spectra of (a) **PTPTPTBT** and (b) **PTPTPTQX** in the chloroform solution and the solid state. Absorption spectrum of **PDIDTDTBT** in chloroform is included in (a) for comparison.

dx.doi.org/10.1021/cm202612t|*Chem. Mater.* 2011, 23, 5068–5075

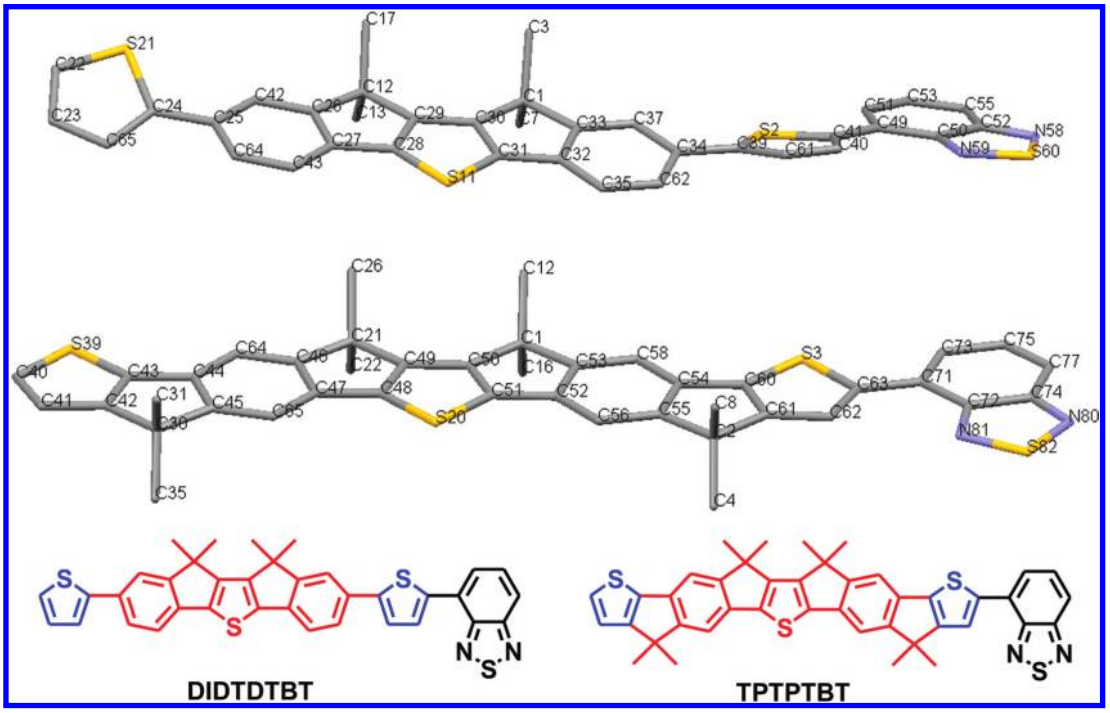

Figure 4. Optimized conformations for the structure of **DIDTDTBT** (top) and **TPTPTBT** (bottom), respectively, at the level of B3LYP/6-31G(d). Yellow: sulfur; blue: nitrogen; and gray: carbon; hydrogens are omitted for clarity.

Figure 5. Wave functions of the HOMO (left) and LUMO (right) orbitals of the **TPTPTBT** calculated at the level of B3LYP/6-31G (d,p).

structural motifs are φ(C40−C41−C49−C50) = 7.32° for **DIDTDTBT** and φ(C62−C63−C71−C72) = 0.07° for **TPTPTBT**.

The frontier orbitals of the model compound **TPTPTBT** were also shown in Figure 5. The electron density of the HOMO for **TPTPTBT** is homogeneously distributed along the nonacyclic donor unit, whereas the electron density of the LUMO is redistributed to the BT acceptor unit. Such an electronic redistribution shows a pronounced intramolecular charge separation between donor and acceptor after excitation. The energy of HOMO−LUMO transition for **TPTPTBT** is calculated to be 631 nm, which is in good agreement with its experimental absorption maximum (628 nm in chloroform).

Electrochemical Properties. Cyclic voltammetry (CV) was employed to examine the electrochemical properties and evaluate the HOMO and LUMO levels of the polymer (Figure 6 and Table 3). Both polymers showed a stable and reversible p-doing and n-doping processes, which are important prerequisites for p-type semiconductor materials. The HOMO energy levels being estimated to be −5.24 eV for **PTPTPTBT** and −5.21 eV for **PTPTPTQX** are in an ideal range to ensure better air-stability and greater attainable V_{oc} in the final device. The LUMO energy levels are approximately located at −3.38 eV for **PTPTPTBT** and −3.30 eV for **PTPTPTQX**, which are higher than the LUMO level of the $PC_{71}BM$ acceptor (−3.8 eV) to ensure energetically favorable electron transfer. This can be unambiguously evidenced by the complete photoluminescence quenching in the film of the

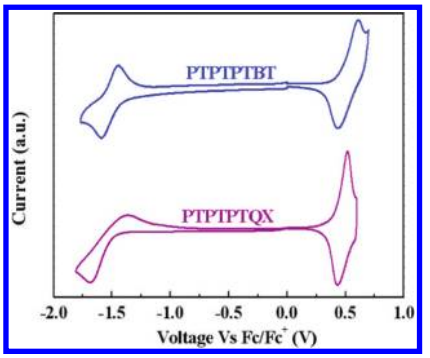

Figure 6. Cyclic voltammograms of **PTPTPTBT** and **PTPTPTQX** in the thin film at a scan rate of 80 mV s^{-1}.

Table 3. Electrochemical Properties of the Polymers

copolymer	E_{ox}^{onset}(V)	E_{red}^{onset}(V)	HOMO (eV)	$LUMO^{el}$ (eV)	E_g^{el} (eV)
PTPTPTBT	0.44	−1.42	−5.24	−3.38	1.86
PTPTPTQX	0.41	−1.50	−5.21	−3.30	1.91

PTPTPTBT/$PC_{71}BM$ (1:4, w/w) and **PTPTPTQX**/$PC_{71}BM$ (1:2, w/w) blends (Figure 7).

Photovoltaic and Hole-Mobility Characteristics. Despite the amorphous nature in thin films, **PTPTPTBT** and **PTPTPTQX** showed good hole transporting properties because of their rigid and coplanar structures. Hole-only

dx.doi.org/10.1021/cm202612t | *Chem. Mater.* 2011, 23, 5068−5075

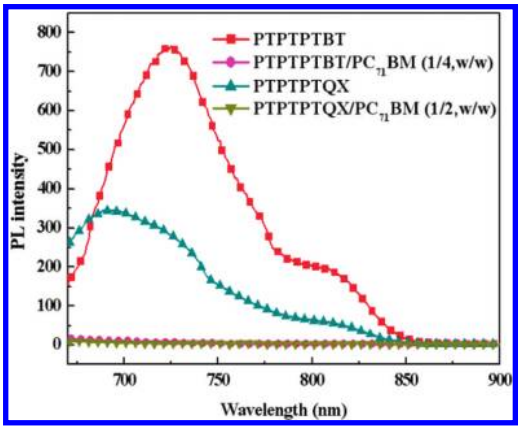

Figure 7. Emission spectra of **PTPTPTBT**, **PTPTPTBT**/$PC_{71}BM$ at excitation wavelength of 628 nm, **PTPTPTQX** and **PTPTPTQX**/$PC_{71}BM$ (1/2, w/w) at excitation wavelength of 593 nm in the thin film.

devices(ITO/PEDOT:PSS/polymer/Au) were fabricated to estimate the intrinsic hole mobilities of these polymers by means of the space-charge limit current (SCLC) theory. **PTPTPTBT** and **PTPTPTQX** exhibited higher hole mobilities of 5.1×10^{-4} $cm^2/(V\,s)$ and 3.7×10^{-4} $cm^2/(V\,s)$, respectively, compared to **PDITIDTBT** with 1×10^{-4} $cm^2/(V\,s)$. On the basis of ITO/PEDOT:PSS/polymer:$PC_{71}BM$/Ca/Al configuration, bulk heterojunction solar cells were fabricated and characterized under simulated 100 mW cm^{-2} AM 1.5 G illumination. The current density–voltage characteristics of the devices are shown in Figure 8 and the device parameters are summarized in Table 4. The preliminary device based on **PTPTPTQX**/$PC_{71}BM$ (1:2, w/w) blend exhibited a V_{oc} of 0.74 V, a J_{sc} of 9.0 mA/cm^2, a FF of 61% and a high PCE of 4.1%. More encouragingly, the device using **PTPTPTBT**/$PC_{71}BM$ (1:4, w/w) blend delivered superior performance with a J_{sc} of 11.4 mA/cm^2, a V_{oc} of 0.76 V, a FF of 61%, and an exceptional PCE of 5.3%, which dramatically outperforms the device based on the nonfused **PDIDTDTBT**/$PC_{71}BM$ (1:2, w/w) blend by 3-fold. (V_{oc} = 0.7 V, J_{sc} = 5.30 mA/cm^2, FF = 44%, and a PCE of 1.65%).[7] This result reveals that the nonacyclic **TPTPT** unit having rigid and extended coplanar conjugated system indeed improves all the device characteristics.

The morphology of thin film was evaluated by atomic force microscopy (Figure 9). The image of the **PTPTPTBT**/$PC_{71}BM$ (1:4, w/w) blend showed a very smooth surface and small phase separation domains, suggesting its good morphological properties for efficient charge separation and transport.

BHJ devices with inverted architecture are known to possess much improved long-term stability compared to conventional structure. However, PCEs of P3HT/PCBM-based inverted PSCs are mostly in the range of *ca.* 2–4%, which is inferior to that of conventional PSCs.[9] Therefore, recent research of inverted solar cells is mainly devoted to device engineering and interfacial modification. The utilization of low bandgap (LBG) conjugated polymers other than P3HT as p-type photoactive materials is only sporadically explored.[10] It is highly desirable to evaluate the new copolymers in the application of inverted solar cells. The inverted devices were fabricated based on the configuration of ITO/ZnO/C-PCBSD/copolymer:$PC_{71}BM$/PEDOT:PSS/Ag where a cross-linked $PC_{61}BM$ derivative, [6,6]-phenyl-C_{61}-butyric styryl dendron ester (C-PCBSD) was used as an interlayer.[11] Encouragingly, the inverted device using **PTPTPTQX**/$PC_{71}BM$ (1:2, w/w) blend delivered an enhanced PCE of 4.7%. Similarly, the device incorporating **PTPTPTBT**/$PC_{71}BM$ (1:4, w/w) blend further achieved a high PCE of 5.9% with J_{sc} = 12.10 mA/cm^2, V_{oc} = 0.76 V and FF = 64%. This performance outperforms not only the P3HT/$PC_{61}BM$-based device under the identical device configuration (PCE = 4.4%)[11] but also an inverted tandem cell (PCE = 5.1%) combining P3HT and poly[bis(2-ethylhexyl)dithienosilole)-*alt*-(2,1,3-benzothiadiazole)] (PSBTBT) as the photoactive materials.[12] To confirm the accuracy of the measurements of the devices, the corresponding external quantum efficiency (EQE) for both the conventional and inverted solar cells was measured under illumination of monochromatic light (Figure 8). The J_{sc} calculated from integration of the EQE with an AM 1.5 G reference spectrum agrees well with the J_{sc} obtained from the J–V measurements.

CONCLUSIONS

In summary, we have successfully synthesized a nonacylic distannyl-**TPTPT** unit that consists of alternate thiophene and benzene units fused by four embedded cyclopentadienyl rings. **PTPTPTBT** and **PTPTPTQX** copolymers incorporating this rigidified and coplanar **TPTPT** units simultaneously possess excellent solubilities for solution-processability, low bandgaps with suitable position of HOMO/LUMO energy levels, and high hole mobilities, leading to promising PCEs of 4.1 and 5.3%, respectively. Most significantly, the **PTPTPTBT**/$PC_{71}BM$-based device with inverted architecture achieved an impressively high PCE of 5.9%. This value is among the highest

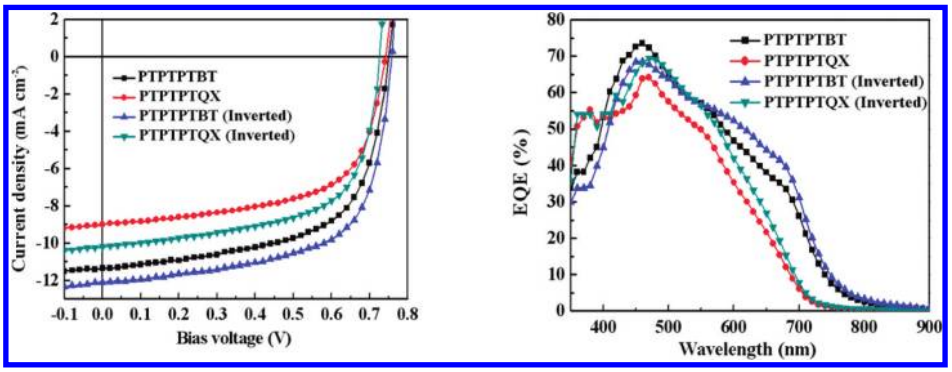

Figure 8. Current density–voltage characteristics (left) and EQE spectra (right) of the conventional devices (ITO/PEDOT:PSS/polymer:$PC_{71}BM$/Ca/Al) and inverted devices (ITO/ZnO/C-PCBSD/polymer: $PC_{71}BM$/PEDOT:PSS/Ag) devices under illumination of AM 1.5 G, 100 mW cm^{-2}.

dx.doi.org/10.1021/cm202612t|*Chem. Mater.* 2011, 23, 5068–5075

Table 4. Hole Mobilities and Photovoltaic Characteristics

copolymer	polymer:$PC_{71}BM$ wt% ratio	mobility (cm^2/V s)	V_{oc} (V)	J_{sc} (mA/cm^2)	FF (%)	PCE (%)
PTPTPTBT[a]	1:4	5.1×10^{-4}	0.76	11.4 (11.2) [c]	61	5.3
PTPTPTBT[b]	1:4		0.76	12.1 (11.6)[c]	64	5.9
PTPTPTQX[a]	1:2	3.7×10^{-4}	0.74	9.0 (9.1) [c]	61	4.1
PTPTPTQX[b]	1:2		0.74	10.2 (9.6) [c]	62	4.7

[a]Conventional device structure: ITO/PEDOT:PSS/copolymer:$PC_{71}BM$/Ca/Al. [b]Inverted device structure: ITO/ZnO/C-PCBSD/copolymer:$PC_{71}BM$/PEDOT:PSS/Ag. [c]Calculated from the EQE spectrum.

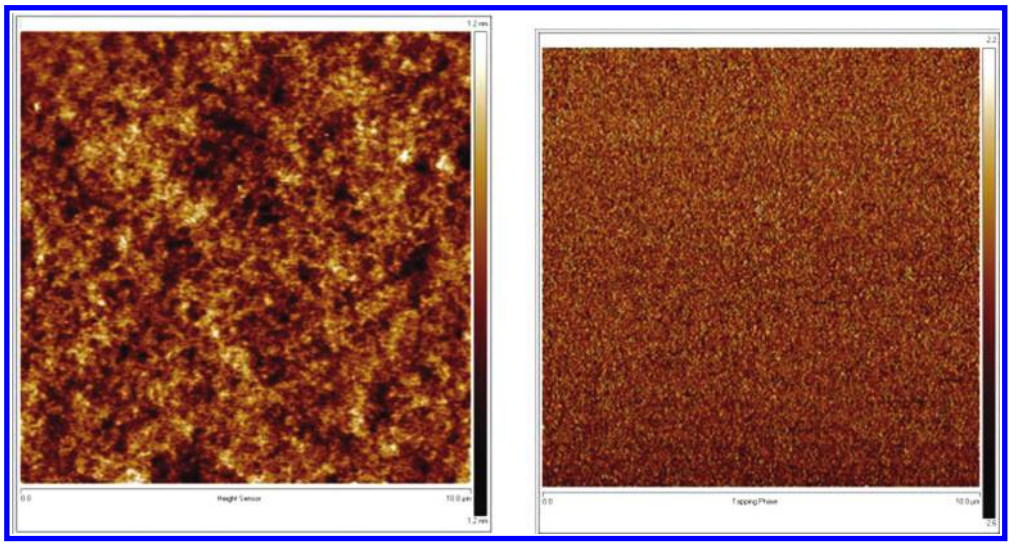

Figure 9. AFM height (left) and phase images (right) of the surface of **PTPTPTBT**/PC71BM (1:4, w/w) blend (10.0 μm × 10.0 μm). The surface roughness is estimated to be 0.4 nm.

efficiency ever reported for the inverted solar cells incorporating a D−A type LBG polymer. We envisage that further improvement of device performance is achievable by optimizing the processing conditions.

EXPERIMENTAL SECTION

General Measurement and Characterization. All chemicals are purchased from Aldrich or Acros and used as received unless otherwise specified. ^1H and ^{13}C NMR spectra were measured using Varian 300 MHz instrument spectrometer. The molecular weight of polymers was measured by the GPC method (Viscotek VE2001GPC), and polystyrene was used as the standard (THF as the eluent). Differential scanning calorimeter (DSC) was measured on TA Q200 Instrument and thermal gravimetric analysis (TGA) was recorded on Perkin-Elmer Pyris under a nitrogen atmosphere at a heating rate of 10 °C/min. Absorption spectra were taken on a HP8453 UV−vis spectrophotometer. The electrochemical cyclic voltammetry was conducted on a CH instruments electrochemical analyzer. A carbon glass coated with a thin polymer film was used as the working electrode and an Ag/AgCl as the reference electrode, whereas 0.1 M tetrabutylammonium hexafluorophosphate ($TBAPF_6$) in acetonitrile was the electrolyte. CV curves were calibrated using ferrocence as the standard, whose HOMO is set at —4.8 eV with respect to zero vacuum level. The HOMO energy levels were obtained from the equation HOMO = $-(E_{ox}^{onset} - E_{(ferrocene)}^{onset} + 4.8)$ eV. The LUMO levels of polymer were obtained from the equation LUMO = $-(E_{red}^{onset} - E_{(ferrocene)}^{onset} + 4.8)$ eV. Surface images were measured by Veeco di-Innova Atomic Force Microscope.

Fabrication and Characterization of BHJ Devices. ITO/Glass substrates were ultrasonically cleaned sequentially in detergent, water, acetone and isopropyl alcohol. Then, the substrates were covered by a 30 nm thick layer of PEDOT:PSS (Clevios P provided by H. C. Stark) by spin coating. After annealing in air at 150 °C during 30 min, the samples were cooled down to rt. Polymers were dissolved in *ortho*-dichlorobenzene (ODCB) (0.47 wt.%) and $PC_{71}BM$ (purchased from Nano-C) was added to reach the desired ratio. The solution was then heated at 110 °C and stirred overnight. Prior to deposition, the solution was filtrated through a 0.45 μm filter and the substrates were transferred in a glovebox. The photoactive layer was then spin coated at different spin coating speed in order to tune its thickness. After drying, the samples were annealed during 15 min. The detailed processing parameters (spin coating speed; annealing temperature) are shown as follows: **PTPTPTBT**/$PC_{71}BM$ (700 rpm; 150 °C) and **PTPTPTQX**/$PC_{71}BM$ (700 rpm; 150 °C). The cathode made of calcium (35 nm thick) and aluminum (100 nm thick) was evaporated through a shadow mask under high vacuum (<1×10^{-6} Torr). Each device is constituted of 4 pixels defined by an active area of 0.04 cm^2. Finally, the devices were encapsulated and $I-V$ curves were measured in air.

For the inverted architecture, a ZnO precursor solution, consisting of 157 mg mL^{-1} zinc acetate dehydrate in 96% 2-methoxy ethanol and 4% ethanolamine, was spin coated onto ITO-coated glass, followed by thermal annealing in air at 300 °C for 10 min to crystallize the film (thickness = ca. 50 nm). Subsequently, PCBSD solution (5 mg mL^{-1} in ortho-dichlorobenzene) was spin coated onto the ZnO layer and the as-cast film was heated at 180 °C for 10 min for thermal cross-linking (thickness = 10 nm). The same process for the active layer in the conventional architecture was used for the inverted devices. The PEDOT:PSS solution diluted with equal volume of isopropyl alcohol and 0.2 wt % of Triton X-100 nonionic surfactant, was then spin coated on top of the active layer, followed by thermal annealing at 120 °C for 10 min (thickness = 60 nm). A silver top electrode (thickness = ca. 150 nm) was then thermally evaporated to complete the inverted device.

Hole-Only Devices. To investigate the respective hole mobility of the different copolymer films, we have prepared unipolar devices following the same procedure except that the active layer is made of pure polymer and the Ca/Al cathode is replaced by evaporated gold (40 nm). The hole mobilities were calculated according to space

dx.doi.org/10.1021/cm202612t|*Chem. Mater.* 2011, 23, 5068−5075

charge limited current theory (SCLC). The $J-V$ curves were fitted according to the following equation

$$J = \frac{9}{8}\varepsilon\mu\frac{V^2}{L^3}$$

Where ε is the dielectric permittivity of the polymer, μ is the hole mobility, and L is the film thickness (distance between the two electrodes)

Synthesis of Compound 2. To a 50 mL round-bottom flask was introduced **1** (2.20 g, 2.29 mmol), ethyl 2-bromothiophene-3-carboxylate (1.24 g, 5.27 mmol), $Pd(PPh_3)_4$ (0.265 g, 0.23 mmol), K_2CO_3 (1.90 g, 13.75 mmol), and Aliquant 336 (0.23 g, 0.57 mmol) in a solution of degassed toluene (17 mL) and degassed H_2O (3.5 mL). The mixture was heated to 90 °C under nitrogen for 72 h. The reaction solution was extracted with ethyl acetate (300 mL × 3) and water (150 mL). The combined organic layer was dried over $MgSO_4$. After removal of the solvent under reduced pressure, the residue was purified by column chromatography on silica gel (hexane/ethyl acetate, v/v, 20/1) and then recrystallized from hexane to give a light yellow solid **2** (2.07 g, 62%); mp: 110 °C; ^{1}H NMR ($CDCl_3$, 300 MHz): δ 7.52 (d, J = 5.6 Hz, 2 H), 7.51−7.30 (m, 6 H), 3.17−3.58 (m, 4 H), 7.23 (d, J = 5.6 Hz, 2 H), 4.20 (q, J = 7.2 Hz, 4 H), 2.09 (t, J = 8.1 Hz, 8 H), 1.40−0.96 (m, 54 H), 0.82 (t, J = 13.4 Hz, 12 H); ^{13}C NMR ($CDCl_3$, 75 MHz): δ 163.4, 152.0, 151.6, 149.9, 144.8, 139.3, 130.0, 128.8, 128.1, 123.6, 123.5, 117.3, 60.4, 55.6 40.2, 31.8, 30.3, 29.6, 29.5, 24.2, 22.6, 14.2, 14.0; MS (FAB, $C_{64}H_{88}O_4S_3$): calcd, 1017.58; found, 1017.

Synthesis of Compound 3. A Grignard reagent was prepared by the following procedure. To a suspension of magnesium turnings (0.8 g, 33.3 mmol) and 3−4 drops of 1,2-dibromoethane in dry THF (20 mL) was slowly added 1-bromo-4-(octyloxy)benzene (8.56 g, 30.0 mmol) dropwise and stirred for 1 h. To a solution of **2** (0.80 g, 0.79 mmol) in dry THF (20 mL) under nitrogen was added freshly prepared 4-(octyloxy)benzene 1-magnesium bromide (20 mL, 7.9 mmol) dropwise at room temperature. The resulting mixture was heated at reflux for 16 h. The reaction solution was extracted with ethyl acetate (150 mL × 3) and water (100 mL). The combined organic layer was dried over $MgSO_4$. After removal of the solvent under reduced pressure, the residue was purified by column chromatography on silica gel (hexane/ethyl acetate, v/v, 100/1) to give a yellow oil **3** (1.17 g, 85%); ^{1}H NMR ($CDCl_3$, 300 MHz): δ 7.24 (d, J = 9.0 Hz, 2 H), 7.17 (d, J = 9.0 Hz, 2 H), 7.16 (d, J = 9.0 Hz, 8 H), 7.09 (d, J = 5.1 Hz, 2 H), 6.94 (s, 2 H), 6.84 (d, J = 9.0 Hz, 8 H), 6.41 (d, J = 5.6 Hz, 2 H), 3.97 (t, J = 6.5 Hz, 8 H), 3.07 (s, 2 H), 1.95−1.60 (m, 16 H), 1.55−0.40 (m, 112 H). ^{13}C NMR ($CDCl_3$, 75 MHz): δ 158.2, 152.5, 149.7, 144.5, 144.1, 140.7, 139.2, 138.8, 131.5, 131.0, 128.9, 123.1, 122.2, 117.9, 113.7, 80.4, 68.0, 55.4, 39.9, 31.9, 31.8, 30.2, 29.7, 29.5, 29.4, 29.3, 29.26, 26.1, 24.1, 22.7, 22.6, 14.1, 14.05. MS (FAB, $C_{116}H_{164}O_6S_3$): calcd, 1750.73; found, 1751.

Synthesis of TPTPT. To a solution of **3** (2.00 g, 1.14 mmol) in boiling acetic acid (116 mL) was added conc. sulfuric acid (3.5 mL) in one portion. The resulting solution was stirred for 18 h at 95 °C and then was extracted with ethyl acetate (500 mL × 3) and water (250 mL). The combined organic layer was dried over $MgSO_4$. After removal of the solvent under reduced pressure, the residue was purified by column chromatography on silica gel (hexane/ethyl acetate, v/v, 100/1) to give an orange oil **TPTPT** (1.58 g, 81%);^{1}H NMR (d8-THF, 300 MHz): δ 7.45 (s, 2 H), 7.34 (d, J = 4.8 Hz, 2H), 7.33 (s, 2 H), 7.12 (d, J = 8.7 Hz, 8H), 6.99 (d, J = 4.8 Hz, 2H), 6.72 (d, J = 8.7 Hz, 8 H), 3.87 (t, J = 6.0 Hz, 8 H), 2.3−2.1 (m, 8 H), 1.50−0.95 (m, 96 H), 0.90−0.70 (m, 24 H). ^{13}C NMR ($CDCl_3$, 75 MHz): δ 157.9, 155.9, 153.2, 152.2, 148.9, 144.6, 141.3, 137.1, 137.0, 134.3, 129.0, 126.9, 123.0, 115.8, 114.1, 113.1, 67.9, 61.8, 55.1, 40.5, 31.9, 31.85, 31.8, 30.3, 29.7, 29.5, 29.3, 29.29, 29.2, 26.0, 24.2, 22.6, 14.1, 14.0. MS (FAB, $C_{116}H_{160}O_4S_3$): calcd, 1714.70; found, 1715.

Synthesis of Sn-TPTPT. To a solution of **TPTPT** (1.60 g, 0.93 mmol) in dry THF (28 mL) was added 1.6 M solution of t-BuLi in hexane (1.8 mL, 2.80 mmol) dropwise at −78 °C. After stirring at −78 °C for 1 h, 1.0 M solution of chlorotrimethylstannane in THF (3.7 mL, 3.73 mmol) was introduced dropwise by syringe to the solution. The mixture solution was quenched with water and extracted with hexane (300 mL × 3) and water (100 mL). The combined organic layer was dried over $MgSO_4$. After removal of the solvent under reduced pressure, Sn-**TPTPT** (1.18 g, 62%) was obtained as an orange oil and used without further purification; ^{1}H NMR ($CDCl_3$, 300 MHz): δ 7.29 (s, 2 H), 7.27 (s, 2H), 7.21 (d, J = 8.7 Hz, 8 H), 7.06 (s, 2 H), 6.81 (d, J = 8.7 Hz, 8 H), 3.94 (t, J = 6.3 Hz, 8 H), 2.20−2.00 (m, 8 H), 1.85−1.70 (m, 8 H), 1.50−0.60 (m, 112 H), 0.40 (s, 18 H). ^{13}C NMR ($CDCl_3$, 75 MHz): 157.8, 153.5, 152.1, 148.8, 147.3, 144.5, 140.5, 137.2, 136.9, 134.1, 130.5, 129.1, 129.0, 115.8, 114.0, 113.2, 67.8, 61.3, 55.0, 40.4, 35.7, 31.8, 31.7, 30.3, 29.6, 29.4, 29.3, 29.2, 26.0, 24.2, 22.6, 14.06, 14.03, −8.0. Elemental anal. Calcd (%) for $C_{122}H_{176}O_4S_3Sn_2$: C, 71.82; H, 8.69. Found: C, 71.67; H, 8.78.

Synthesis of PTPTPTBT. To a 15 mL round-bottom flask was introduced Sn-**TPTPT** (145.4 mg, 0.07 mmol), 4,7-dibromo-2,1,3-benzothiadiazole **BT** (20.6 mg, 0.07 mmol), $Pd_2(dba)_3$ (3.2 mg, 0.0035 mmol), tri(*o*-tolyl)phosphine (6.8 mg, 0.022 mmol), and dry chlorobenzene (3 mL). The mixture was then degassed by bubbling nitrogen for 10 min at room temperature. The round-bottom flask was placed into the microwave reactor and reacted for 45 min under 270 W. To end-cap the resulting polymer, we added tributyl(thiophen-2-yl)stannane (13.1 mg, 0.035 mmol) to the mixture solution and reacted it for 10 min under 270 W. Finally, 2-bromothiophene (6.2 mg, 0.038 mmol) was added to the mixture solution and reacted for 10 min under 270 W. The solution was added into methanol dropwise. The precipitate was collected by filtration and washed by Soxhlet extraction with acetone, hexane, and chloroform sequentially for one week. The Pd-thiol gel (Silicycle Inc.) and Pd-TAAcOH were added to above chloroform solution to remove the residual Pd catalyst and Sn metal. After filtration and removal of the solvent, the polymer was redissolved in chloroform again and added into methanol to reprecipitate. The purified polymer was collected by filtration and dried under vacuum for 1 day to give a dark-green fiber-like solid (215 mg, 62%, M_n = 30 000, PDI = 1.69). ^{1}H NMR ($CDCl_3$, 300 MHz): δ 8.20−8.00 (m, 2 H), 7.95−7.80 (m, 2 H), 7.50−7.30 (m, 4 H), 7.25−7.15 (m, 8 H), 6.90−6.70 (m, 8 H), 4.00−3.80 (m, 8H), 1.85−1.60 (m, 16H), 1.50−1.00 (m, 88 H), 0.90−0.70 (m, 24 H

Synthesis of PTPTPTQX. To a 15 mL round-bottom flask was introduced Sn-**TPTPT** (259.7 mg, 0.13 mmol), 5,8-dibromo-2,3-diphenylquinoxaline **QX** (56 mg, 0.13 mmol), $Pd_2(dba)_3$ (4.7 mg, 0.0051 mmol), tri(*o*-tolyl)phosphine (12.4 mg, 0.041 mmol) and dry chlorobenzene (5 mL). The mixture was then degassed by bubbling nitrogen for 10 min at room temperature. The round-bottom flask was placed into the microwave reactor and reacted for 45 min under 270 W. To end-cap the resulting polymer, tributyl(thiophen-2-yl)stannane (23.8 mg, 0.064 mmol) was added to the mixture solution and reacted for 10 min under 270 W. Finally, 2-bromothiophene (11.2 mg, 0.069 mmol) was added to the mixture solution and reacted for 10 min under 270 W. The solution was added into methanol dropwise. The precipitate was collected by filtration and washed by Soxhlet extraction with acetone, hexane, and chloroform sequentially for one week. The Pd-thiol gel (Silicycle Inc.) and Pd-TAAcOH were added to above chloroform solution to remove the residual Pd catalyst and Sn metal. After filtration and removal of the solvent, the polymer was redissolved in chloroform again and added into methanol to reprecipitate. The purified polymer was collected by filtration and dried under vacuum for 1 day to give a dark-green fiberlike solid (155 mg, 61%, M_n = 34 000, PDI = 1.60). ^{1}H NMR ($CDCl_3$, 300 MHz): δ 8.10−8.00 (m, 2H), 7.95−7.85 (m, 2H), 7.80−7.70 (m, 4H), 7.55−7.30 (m, 10H), 7.20−7.00 (m, 8H), 6.90−6.70 (m, 8H), 4.00−3.80 (m, 8H), 1.85−1.65 (m, 16H), 1.50−1.00 (m, 88 H), 0.90−0.70 (m, 24 H).

■ ASSOCIATED CONTENT

Ⓢ Supporting Information

^{1}H and ^{13}C NMR spectra. This material is available free of charge via the Internet at http://pubs.acs.org.

AUTHOR INFORMATION

Corresponding Author

*E-mail: yjcheng@mail.nctu.edu.tw (Y.-J.C.); cshsu@mail.nctu.edu.tw (C.-S.H.).

ACKNOWLEDGMENTS

This work was supported by the National Science Council and "ATP Plan" of the National Chiao Tung University and Ministry of Education, Taiwan. We thank Yi-Lin Wu for the help of theoretical calculations.

REFERENCES

(1) (a) Yu, G.; Gao, J.; Hummelen, J. C.; Wudl, F.; Heeger, A. J. *Science* **1995**, *270*, 1789. (b) Thompson, B. C.; Fréchet, J. M. J. *Angew. Chem., Int. Ed.* **2008**, *47*, 58. (c) Günes, S.; Neugebauer, H.; Sariciftci, N. S. *Chem. Rev.* **2007**, *107*, 1324. (d) Cheng, Y.-J.; Yang, S.-H.; Hsu, C.-S. *Chem. Rev.* **2009**, *109*, 5868. (e) Chen, J.; Cao, Y. *Acc. Chem. Res.* **2009**, *42*, 1709.

(2) (a) Price, S. C.; Stuart, A. C.; Yang, L.; Zhou, H.; You, W. *J. Am. Chem. Soc.* **2011**, *133*, 4625. (b) Piliego, C.; Holcombe, T. W.; Douglas, J. D.; Woo, C. H.; Beaujuge, P. M.; Fréchet, J. M. J. *J. Am. Chem. Soc.* **2010**, *132*, 7595. (c) Li, Z.; Ding, J.; Song, N.; Lu, J.; Tao, Y. *J. Am. Chem. Soc.* **2010**, *132*, 13160. (d) Chu, T.-Y.; Lu, J.; Beaupré, S.; Zhang, Y.; Pouliot, J.-R.; Wakim, S.; Zhou, J.; Leclerc, M.; Li, Z.; Ding, J.; Tao, Y. *J. Am. Chem. Soc.* **2011**, *133*, 4250. (e) Chen, H.-Y.; Hou, J.; Zhang, S.; Liang, Y.; Yang, G.; Yang, Y.; Yu, L.; Wu, Y.; Li, G. *Nat. Photon.* **2009**, *3*, 649. (f) Wang, M.; Hu, X.; Liu, P.; Li, W.; Gong, X.; Huang, F.; Cao, Y. *J. Am. Chem. Soc.* **2011**, *133*, 9638.

(3) (a) Svensson, M.; Zhang, F.; Veenstra, S. C.; Verhees, W. J. H.; Hummelen, J. C.; Kroon, J. M.; Inganäs, O.; Andersson, M. R. *Adv. Mater.* **2003**, *15*, 988. (b) Zhou, Q.; Hou, Q.; Zheng, L.; Deng, X.; Yu, G.; Cao, Y. *Appl. Phys. Lett.* **2004**, *84*, 1653. (c) Zhang, F.; Perzon, E.; Wang, X.; Mammo, W.; Andersson, M. R.; Inganäs, O. *Adv. Funct. Mater.* **2005**, *15*, 745.

(4) (a) Zhu, Z.; Waller, D.; Gaudiana, R.; Morana, M.; Mühlbacher, D.; Scharber, M.; Brabec, C. *Macromolecules* **2007**, *40*, 1981. (b) Mühlbacher, D.; Scharber, M.; Zhengguo, M. M.; Zhu, M. M. Z.; Waller, D.; Gaudiana, R.; Brabec, C. *Adv. Mater.* **2006**, *18*, 2884. (c) Chen, C.-H.; Hsieh, C.-H.; Dubosc, M.; Cheng, Y.-J.; Hsu, C.-S. *Macromolecules* **2010**, *43*, 697.

(5) (a) Roncali, J. *Macromol. Rapid Commun.* **2007**, *28*, 1761.

(6) (a) Brédas, J. L.; Calbert, J. P.; da Silva Filho, D. A.; Cornil. *J. Proc. Natl. Acad. Sci. USA* **2002**, *99*, 5804. (b) Ando, S.; Nishida, J.-I.; Tada, H.; Inoue, Y.; Tokito, S.; Yamashita, Y. *J. Am. Chem. Soc.* **2005**, *127*, 5336.

(7) (a) Zhang, Y.; Zou, J.; Yip, H.-L.; Chen, K.-S.; Davies, J. A.; Sun, Y.; Jen, A. K.-Y. *Macromolecules* **2011**, *44*, 4752. (b) Zhang, M.; Guo, X.; Wang, X.; Wang, H.; Li, Y. *Chem. Mater.* **2011**, *23*, 4264. (c) Chen, Y.-C.; Yu, C.-Y.; Fan, Y.-L.; Hung, L.-I.; Chen, C.-P.; Ting, C. *Chem. Commun.* **2010**, *46*, 6503.

(8) Chen, C.-H.; Cheng, Y.-J.; Dubosc, M.; Hsieh, C.-H.; Chu, C.-C.; Hsu, C.-S. *Chem. Asian. J.* **2010**, *5*, 2483.

(9) (a) Mor, G. K.; Shankar, K.; Paulose, M; Varghese, O. K.; Grimes, C. A. *Appl. Phys. Lett.* **2007**, *91*, 152111. (b) Waldauf, C.; Morana, M.; Denk, P.; Schilinsky, P.; Coakley, K.; Choulis, S. A.; Brabec, C. J. *Appl. Phys. Lett.* **2006**, *89*, 233517. (c) White, M. S.; Olson, D. C.; Shaheen, S. E.; Kopidakis, N.; Ginley, D. S. *Appl. Phys. Lett.* **2006**, *89*, 143517. (d) Steim, R.; Choulis, S. A.; Schilinsky, P.; Brabec, C. J. *Appl. Phys. Lett.* **2008**, *92*, 093303. (e) Liao, H.-H.; Chen, L.-M.; Xu, Z.; Li, G.; Yang, Y. *Appl. Phys. Lett.* **2008**, *92*, 173303. (f) Hau, S. K.; Yip, H.-L.; Acton, O.; Baek, N. S.; Ma, H.; Jen, A. K.-Y. *J. Mater. Chem.* **2008**, *18*, 5113.

(10) (a) Wang, T.; Cai, W.; Qin, D.; Wang, E.; Lan, L.; Gong, X.; Peng, J.; Cao, Y. *J. Phys. Chem. C* **2010**, *114*, 6849. (b) Zhang, Y.; Hau, S. K.; Yip, H.-L.; Sun, Y.; Acton, O.; Jen, A. K.-Y. *Chem. Mater.* **2010**, *22*, 2696. (c) Amb, C. M.; Chen, S.; Graham, K. R.; Subbiah, J.; Small, C. E.; So, F.; Reynolds, J. R. *J. Am. Chem. Soc.* **2011**, *133*, 10062.

(11) (a) Hsieh, C.-H.; Cheng, Y.-J.; Li, P.-J.; Chen, C.-H.; Dubosc, M.; Liang, R.-M.; Hsu, C.-S. *J. Am. Chem. Soc.* **2010**, *132*, 4887. (b) Cheng, Y.-J.; Hsieh, C.-H.; He, Y.; Hsu, C.-S.; Li, Y. *J. Am. Chem. Soc.* **2010**, *132*, 17381.

(12) Chou, C.-H.; Kwan, W. L.; Hong, Z.; Chen, L.-M.; Yang, Y. *Adv. Mater.* **2011**, *23*, 1282.